Atomic Order Evaluation of Aging Degradation Process Involving Diffusional Transport of Atoms in Nanometer Scale Regions

Yuichi Ishikawa and Toshihiko Yoshimura

Mechanical Engineering Research Laboratory, Hitachi, Ltd.
502 Kandatsu, Tsuchiura, Japan 300

(Received: Jan. 31, 1997 Accepted: Mar. 7, 1997)

Abstract

Diffusional Transport of atoms and resulting chemical composition changes in nanometer scale regions are often involved in the process of aging degradation of structural materials. The three dimensional atom probe was used to evaluate the diffusional transport of atoms occurring in nanometer scale domains by phase separation of ferrite during a long term intermediate temperature aging of a duplex stainless steel and by directional coarsening of γ' phase in a nickel based superalloy single crystal during an early period of high temperature creep.

The true uniqueness of the three dimensional atom probe is demonstrated by the three dimensional visualization of the fine scale microstructure evolution during the aging at the atomic level.By aging at 450°C for up to 5000h, the ferrite phase of a 25Cr-6Ni-3Mo ferritic/austenitic duplex stainless steel undergoes phase separation by spinodal decomposition, evolving a ultra-fine scale highly interconnected microstructure consisting of the Cr-enriched α' domains and the Cr-depleted Fe-rich α domains. The precipitation of α' phase is responsible for embrittlement and the formation of the Cr-depleted α domains for loss of corrosion resistance.During the initial stage of high temperature creep of a nickel based superalloy single crystal diffusion transport of aluminum atoms gives rise to the formation of nanometer size ordered structures in the disordered matrix channel vertical to the loading axis. Aluminum atoms diffuse from the Al-rich γ' phase through the dislocation cores created at the γ/γ' interface vertical to the loading axis. These fine Al-rich regions form the ordered γ' and coalescence of the precipitates occur. Thus the γ/γ' interface moves in the vertical γ matrix channel which eventually diminishes, resulting in rafting.

1. Introduction

Aging degradation of structural materials is of crucial engineering importance in maintaining high operation efficiency and reliability and extending the life of power generating plant components. Many phenomena in aging degradation of materials depend in some way on diffusion. Common examples are oxidation, creep, precipitation and phase transformations. The recently evolved aging problems in structural materials employed in power generating plants are associated with diffusional transport of atoms and resulting chemical composition changes in nanometer scale regions, such as intermediate temperature embrittlement of duplex stainless steels, high temperature creep of nickel based superalloy single crystals and radiation induced intergranular stress corrosion cracking of stainless steels.

Atomic scale understanding of the degradation process is required to find out why they degrade and how we can prevent the failure. In this paper we will demonstrate the true uniqueness of three dimensional (3D) atom probe, position sensitive atom probe (PoSAP) and show how we have applied it to visualize the aging degradation process of a duplex stainless steel and a nickel based superalloy single crystal.In the ferritic/austenitic duplex stainless steel, diffusional transport of atoms and resulting chemical composition changes in nanometer scale domains lead to the phase separation of the ferritic phase and evolution of the very fine scale interconnected microstructure during a long term exposure at intermediate temperatures as low as 300°C. As a result hardening and embrittlement of the steel occur similar to 475°C embrittlement, accompanied with loss of corrosion resistance and magnetic property change. In the nickel based superalloy single crystal, a directional coarsening of the initially cuboidal γ' phase, often termed as rafting, occurs during the initial stage of high temperature creep above 900°C. The rafting eventually dictates the usable life of the alloy.

2. Atomic order evaluation techniques

The recent progress in atomic order evaluation has enabled us to see, to identify and even to manipulate a single atom. Table 1 shows a list of techniques which can be used for atomic order evaluation. While transmission electron microscope and scanning tunneling microscope

Table 1 Comparison between atomic order evaluation techniques

	Specimen	Resolution	Elemental identification	Depth resolution
AP	sharp needle	single atom	atom by atom	one atomic layer
STM	flat plate	single atom	developing	a tenth of Å
TEM	thin foil	single atom	10Å	averaged over foil thickness

are mostly used for observing a single atom in the periodic atomic configurations, the true uniqueness of the atom probe comes from its ability to identify a single atom. This single atom detection sensitivity may be used to investigate the atomic scale chemistry of the aging degradation process.

Atom probe consists of an field ion microscope and time-of-flight mass spectrometer equipped with a detector that has single atom sensitivity. Figure 1 illustrates the principle of operation of the position sensitive atom probe (PoSAP) which is a recent addition to variants of the atom probe.[1] The operation is based on the process of field evaporation which makes three-dimensional structural and chemical analysis possible with the atom probe. The most prominent surface atoms are field evaporated by applying a slightly higher voltage to a sharp needle-like specimen called tip than that required for producing a field-ion image in the form of a series of high voltage pulses with nanosecond rise time.

Field evaporation removes atoms from the surface in a form of positively charged ions which are repelled and projected approximately radially towards the position sensitive detector placed typically 100–500mm from the specimen. The position sensitive detector is composed of a double microchannel plate and a wedge-and-strip anode. The time-of-flight that the ion takes to travel a distance from the specimen to the detector is measured by a high-speed timing system. The mass-to-charge ratio of the ion, m/n, is calculated by equating the potential energy of the atom on the specimen to the kinetic energy that the atom acquires immediately after field evaporation. The elemental identity of each ion is finally determined from the mass-to-charge ratio. The x and y positions of each ion striking the detector are determined from the relative charges measured on the X, Y and Z electrodes of the wedge-and-strip anode. Although the atom probe has no mass limitations and is equally sensitive to all elements, the wide acceptance angle design without energy compensation has limited mass resolutions, $m/\Delta m$, to 50–250. Furthermore the accurate position of the ion impact is obtained only when a single ion of a given species strikes the detector on any field evaporation pulses. This single-ion-per-pulse constraint has been overcome by a recent development of multianode detector arrays with parallel time recording systems.[2)–4)] In addition the mass resolution of the position sensitive atom probe has been improved to $m/\Delta m \simeq 500$ by incorporating an energy compensating reflectron.[5)]

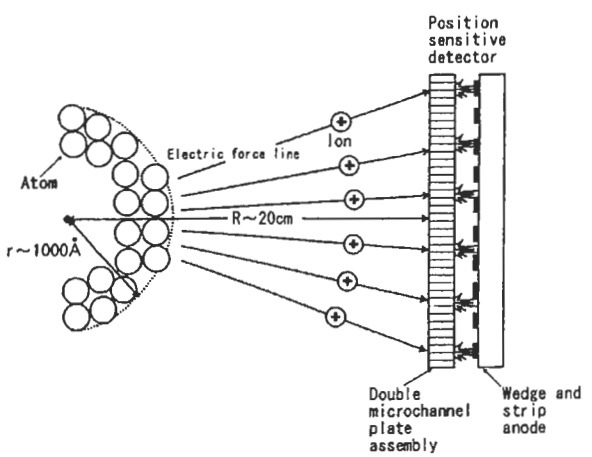

Fig. 1 Principle of operation of the position sensitive atom probe (PoSAP)

Successive field evaporation of the surface atoms produces a two dimensional atom map with respect to time for a region of approximately 15~30nm in diameter. Time sequences of the atom map obtained are expanded into the three dimensional atom map by estimating the depth of field evaporated atomic layers from the applied voltage, the lattice constant and the specimen radius. Thus the composition of a nanometer scale region is determined by simply collecting and identifying the atoms in that volume of material. Subsequent processing can be performed on a graphic software as described by Cerezo et al.[6)]

3. Intermediate temperature aging degradation of duplex stainless steels

Ferritic/austenitic duplex stainless steels have long been used for components and piping in power generating, oil and chemical industries because of their excellent corrosion resistance and high fracture toughness. Experimental results obtained in the past fifteen years[7)-10)] have identified a significant potential of embrittlement for the duplex stainless steels that were aged at intermediate temperatures between 300 and 500°C for times up to 70,000h. It has been established for the cast duplex stainless steels (CF3, CF8 and CF8M)[11)] that the ferrite spinodally decomposes during aging between 300 and 400°C to form a Cr-enriched α' phase and an Fe-rich α phase. This is now the generally agreed main mechanism for the aging degradation in mechanical properties, especially the loss of ductility.

Figure 2 shows the hardness measurements for the ferrite phase of 25Cr-6Ni-3Mo duplex stainless steel as a function of aging time at 450°C. The hardness increases greatly in the early stage of aging and then gradually becomes saturated after 1000h. The aging for over 5000h appears to cause softening indicating some overaging. Little change in hardness was noted in the austenite by aging. The compositions presented in Fig.3 were obtained by x-ray spectra as a function of aging time at 450°C. For each specimen, the compositions reported for the ferrite and the austenite represent averages over data obtained on 10 grains of each phase. In view of micrometer level analysis no significant composition change was observed for either ferrite or austenite by aging. Chromium and molybdenum are preferentially partitioned to the ferrite phase, while nickel is partitioned to the austenite phase. For the aged specimen electrolytic etching shows a very smooth uniform dissolution in the austenite phase while fine and localized attack is shown in the ferrite phase, as shown in the SEM micrographs of Fig.4. The x-ray spectra were taken at the white spots shown in Fig.4 for both austenite/ferrite interface and ferrite/ferrite interface. The results are shown in Fig.5. No significant variation of chromium, nickel and molybdenum concentration was observed with location in the grains for either ferrite or austenite. Since the electron beam used for x-ray analysis is about 0.2μm, this suggests that the localized change in the composition of the ferrite phase must be restricted in the

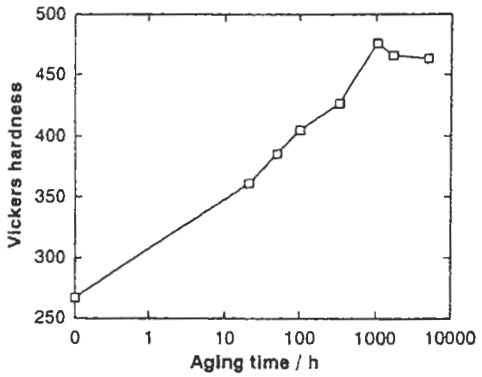

Fig. 2 Microvickers hardness change in the ferrite phase with aging at 450°C

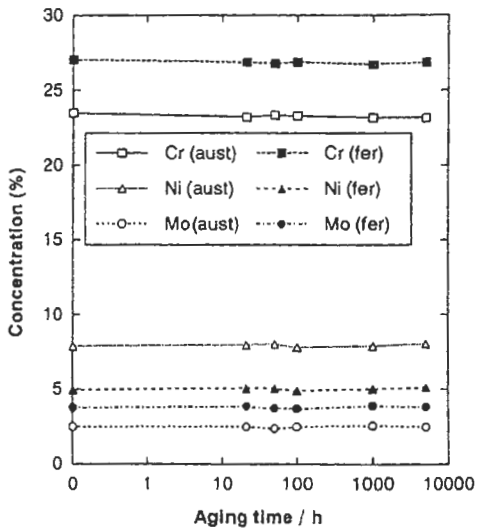

Fig. 3 Chemical compositions of the two phases as a function of aging time at 450°C

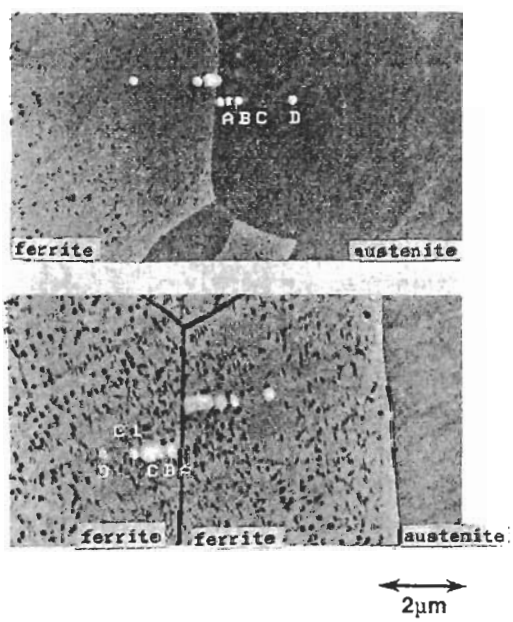

Fig. 4 Comparison of the SEM micrographs between the austenite and ferrite aged for 5000h (electrolytic etching in oxalic acid)

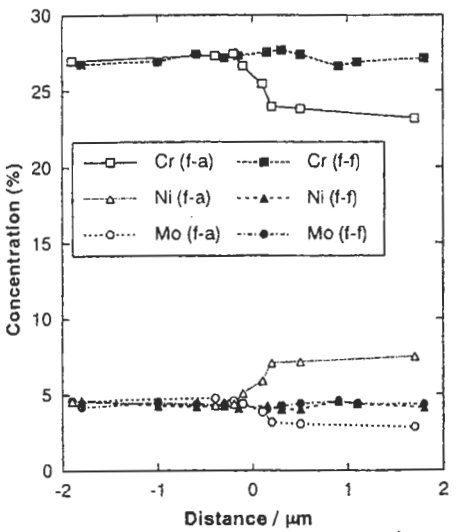

Fig. 5 Chemical composition variation across the austenite / ferrite (open symbols) and ferrite / ferrite (solid symbols) interface. The x-ray spectra were taken at the white spots shown in Fig.4

nanometer range.

Figure 6 shows an example of the two dimensional chromium atom map obtained from the ferrite phase by the PoSAP as a function of aging time at 450°C. This figure represents chromium atoms contained in a sliced cross-section of 15nm in diameter and 1nm thickness. This is the simplest and most intuitive representation of PoSAP data. In the unaged steel, chromium atoms are randomly distributed. Aging for 100h shows the segregation of chromium atoms and further aging shows the enlargement of segregated areas and more concentration of chromium. But each area is only a few nanometer thick. This is accompanied with the formation of the Cr-depleted Fe-rich domains, which are more clearly viewed in the gray scale representation of the sliced section as shown in Fig.7. This is shown to quantitatively view the compositional development of the Cr-enriched and the Cr-depleted domains. Here the compositions are gray scale coded, in which the range of color is mapped to the composition values, that is, from black representing Cr-depleted regions of 12at% Cr or less through gray to white

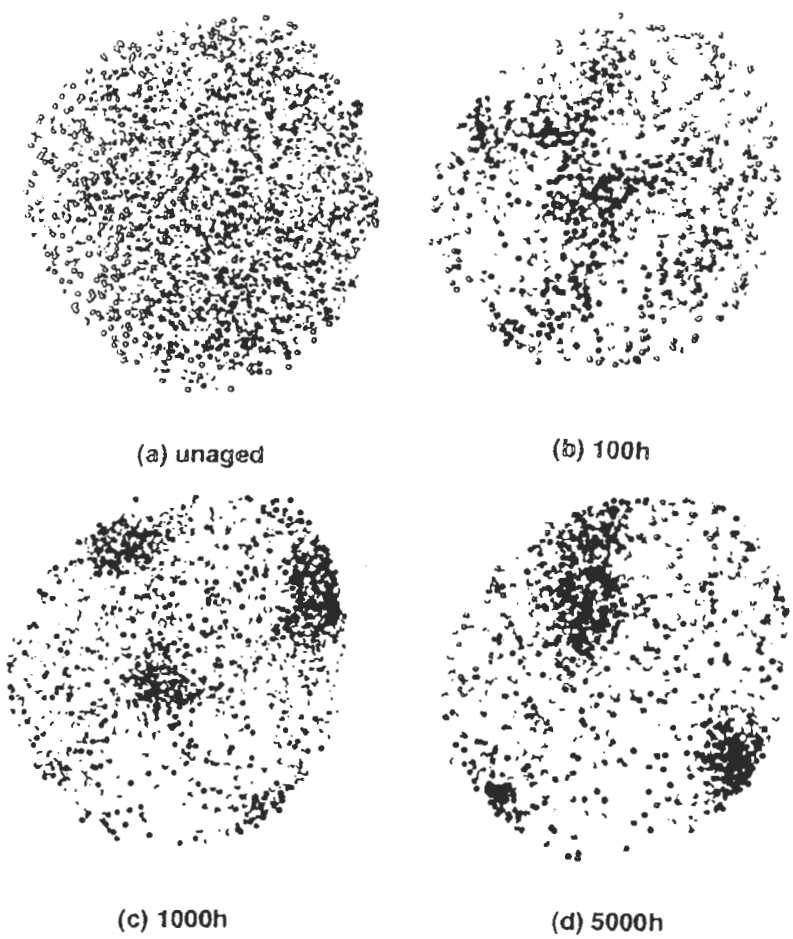

Fig. 6 Example of chromium atom map (Atoms contained in a sliced cross-section of 15nm in diameter and 1nm in thickness)

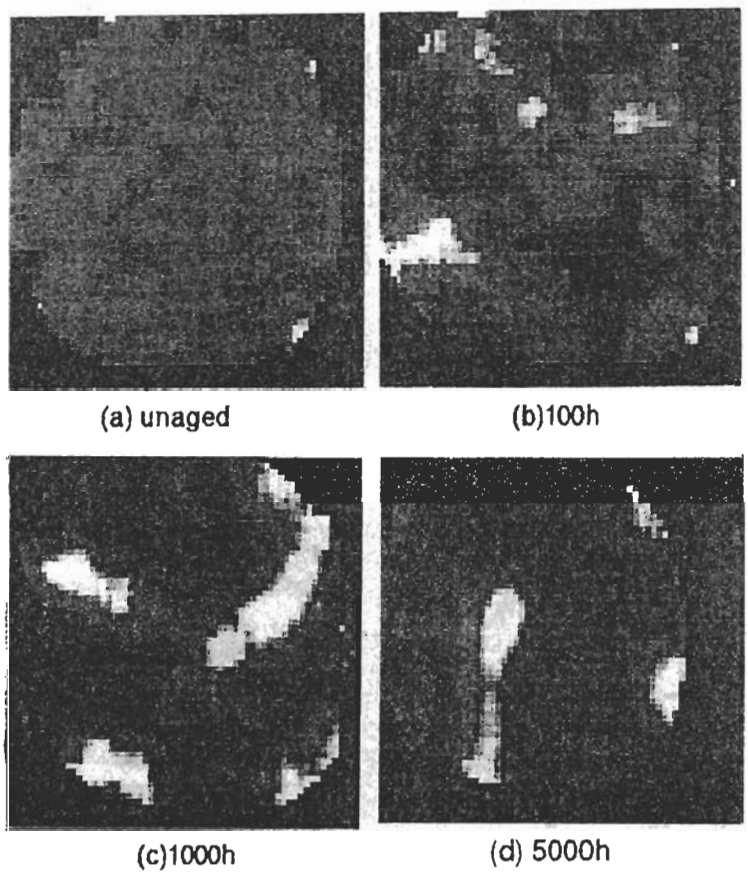

Fig. 7 Gray scale representation of the sliced section shown in Fig.6 (Black represents the Cr-depleted regions of 12at% or less and white does the Cr-enriched regions of 60at% or higher)

representing Cr-enriched regions of 60at% or higher. Aging for 100h causes the formation of the isolated Cr-enriched and Cr-depleted area of a few-nanometer thick and the prolonged aging results in the expansion and interconnection of these areas. Based on these composition cross-section maps, the compositions in each gray scaled area are determined and the result is shown in Fig.8. In addition to the chromium concentration variation, nickel concentration variation should be noted. Nickel concentration tends to increase in the Cr-depleted area and to decrease in the Cr-enriched area. This suggest that nickel is excluded from the Cr-enriched areas and absorbed in the Cr-depleted areas.The average composition in the Cr-depleted area for the steel aged for 5000h is 11.8Cr-8.0Ni-2.7Si-1.2Mo (at%), while that in the Cr-enriched area is 65Cr-3.3Ni-1.4Si-3.0Mo (at%). Loss of corrosion resistance of the steel is attributed to the Cr-depleted domains[12] and loss of ductility to the Cr-enriched domains.[13]

Chromium concentration profiles measured by a conventional energy compensated atom probe are shown in Fig.9.[14] In the early stage of aging

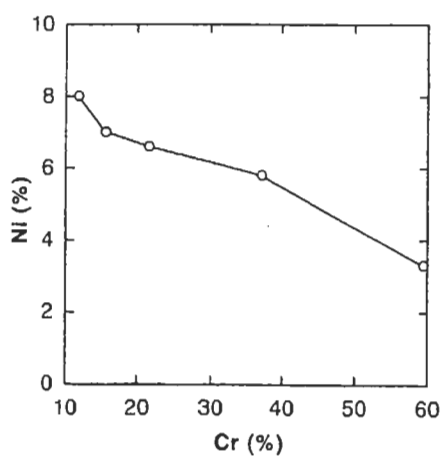

Fig. 8 Nickel concentration change in the gray scaled area with chromium concentration

a small concentration fluctuation is evident. At later stages of aging, well defined sinusoidal type concentration modulations are seen. A frequency distribution for chromium concentration from the PoSAP measurement is constructed by dividing the sequence of atom into equal sized blocks of 50 atoms, calculating the chromium concentration of each block and plotting the observed number of blocks with

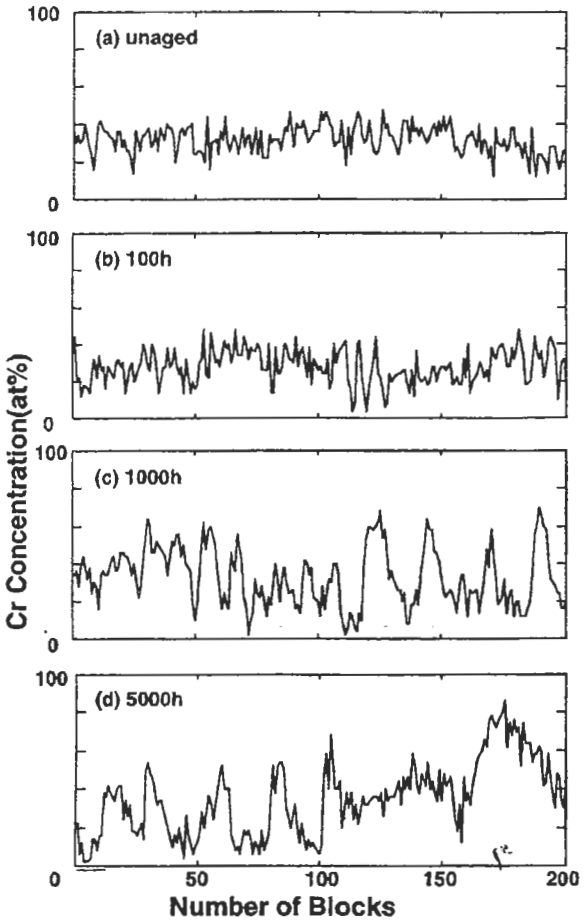

Fig. 9 Chromium concentration profiles measured by a conventional energy compensated atom probe

each chromium concentration. The development of the frequency distribution is shown in Fig.10. A random solution will generate a binomial form, which is the case for the unaged steel (a), whereas a system in which phase separation has occurred will exhibit a broadening of this distribution as in the aged for 100h (b). In the limiting case, a heavily separated sample will yield a distribution with two peaks corresponding to the development of two separated phases as in the aged over 1000h, (c) and (d).

In order to visualize the morphology of the microstructure evolved in the ferrite phase, the isosurface 3D reconstruction of the Cr-enriched domains is presented in Fig.11. The isosurface is the 3D equivalent of a contour. The surface of the Cr-enriched domains are drawn through all points of chromium concentration at 60at%. At a short aging time, the Cr-enriched domains occur as a dispersion of isolated particles, whereas at a longer aging time, the structure has a highly interconnected form.

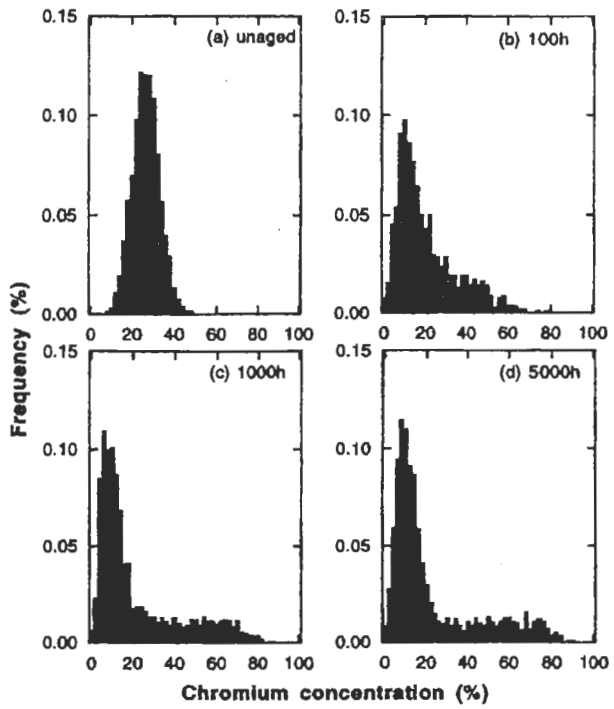

Fig. 10 Frequency distribution for chromium concentration as a function of aging time

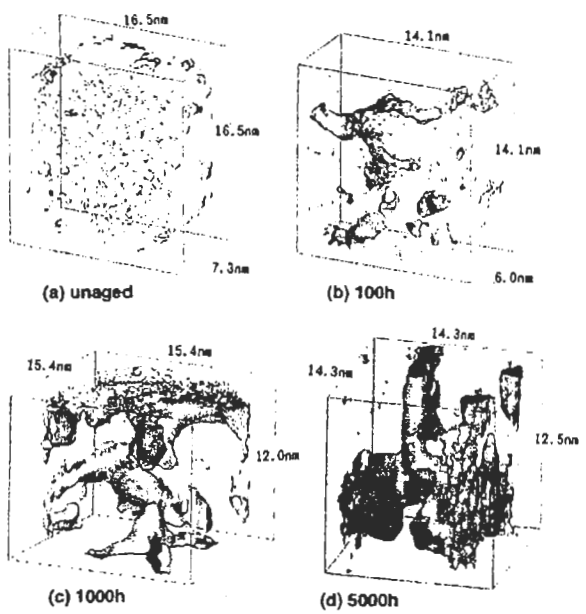

Fig. 11 Isosurface reconstruction showing how the morphology of the Cr-enriched domains evolves. The isosurface is drawn at a chromium concentration of 60at%

4. Precipitation of ultrafine γ' particles in the early period of directional coarsening of a nickel based superalloy single crystal

The continually increasing efficiency, durability and performance of land-based gas turbines require new materials exhibiting high mechanical resistance at elevated temperature. The development of nickel-based superalloy single crystals has led to the manufacture of turbine components exhibiting excellent high temperature creep and fatigue resistance. The typical microstructure of nickel-based superalloy consists of γ' precipitates in a matrix of γ of 0.1μm wide. The initially discrete cuboidal γ' particles directionally coarsen during elevated temperature creep testing to form continuous γ' lamellae, so called rafts, as schematically illustrated in Fig.12.

Since these rafts are believed to influence the creep resistance of the materials, extensive works have been devoted to clarify the detailed mechanism of raft formation and to evaluate the interrelationship among microstructure, composition and creep resistance. This directional coarsening behavior has frequently been related to the elastic interaction between the internal stresses at the γ-γ' interface combined with directed diffusional processes and dislocation behavior caused by lattice mismatch and the applied external load. Compared with extensive studies on lattice mismatch and dislocation texture,[15)–20)] few reports have dealt with elemental diffusional behavior in the early period of rafting.[21)–23)] Without this, it is difficult to understand the physics of the coarsening mechanism. In this section we will visualize the evolution of ultrafine γ' particles in the vertical channel of γ matrix as well as the diffusional transport of a γ'-forming aluminum across the γ-γ' interface in the micro-volume at the initial stage of rafts formation.

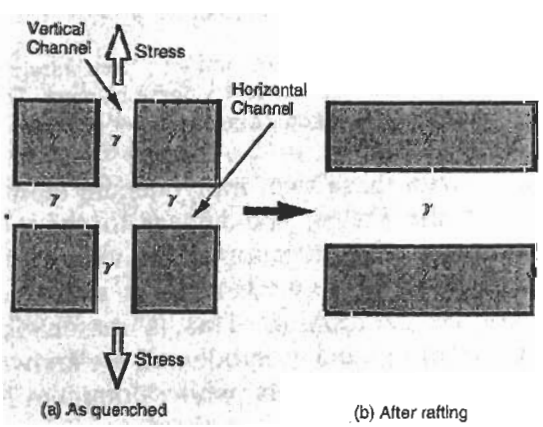

Fig. 12 Schematic illustration of directional coarsening (rafting)

The chemical composition of the specimen for the atom probe analysis is Ni-7.47wt%Cr-7.02wt%W-0.96wt%Mo-1.55at%Re-5.0wtAl-1.68wt%Nb-8.01wt%Ta-0.92wt%Co-0.10wt% Hf. After the solution treatment at 1305°C for 4h, the alloy was aged by two step heat treatment in air at 1040°C for 4h and at 870°C for 20h. The specimens were creep tested in air under uniaxial constant load of 137mPa at 1040°C along [010]. After 2h, the creep test was interrupted and the specimen was forced air quenched. The specimen is believed to be in the initial region of the whole creep curve, where the creep fracture of this alloy occurs in the range between 600h and 800h.

The γ' phase has the L12 ordered structure and is rich in aluminum, while the γ phase is disordered and rich in chromium. Along the [100]crystal direction, the nickel plane and the nickel and aluminum plane are located one by one. Therefore, if the atom probe analysis is carried out along the [100], the layer by layer plane is visualized three dimensionally as shown in Fig.13. This result is supplied by the higher spatial resolution in the depth direction than in the lateral direction on the field evaporation. In Fig.13 only nickel atom is represented by a black dot in the as quenched crystal. It is found that the layer by layer structure of γ' phase shown in Fig.13 does not

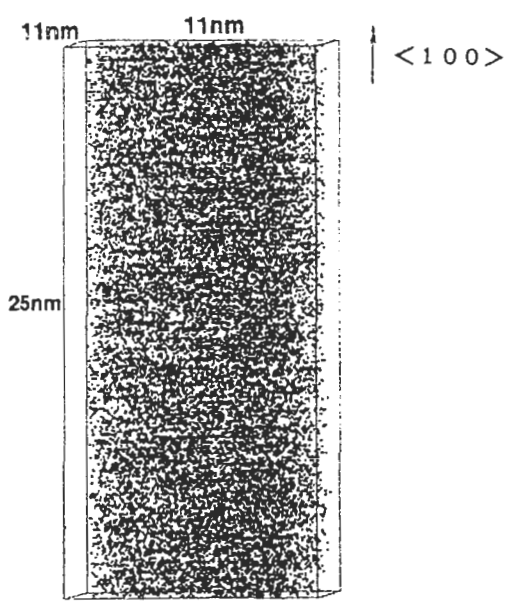

Fig. 13 Nickel atom distribution in the γ' phase

change even after creep testing for 2h.

Figure 14 shows 3D morphology of ultrafine Al-rich precipitates evolved in the vertical γ matrix. This is an isosurface image of aluminum higher than 20at%. The precipitates appear to be very fine when they are located far from the γ-γ' interface and tend to coarsen in the vicinity of the interface. The composition of the Al-rich precipitates is 26.9Al-2.3Cr (at%), which is close to that of the γ' phase (28.2Al-3.6Cr) and surrounded by the Cr-rich domains which have a similar composition (3.1Al-22.4Cr) to the original γ phase (5.0Al-23.1Cr). In order to clearly visualize these domains, the cuboidal small volume of 3nm×3nm×3nm is positioned in a Al-rich precipitate and a Cr-rich domain. The results are shown in Fig.15. The Cr-rich region is regarded as the disordered structure from the arrangement of nickel and aluminum atom (Fig.15 (a)). On the other hand the Al-rich precipitate has the same atomic arrangement as the γ' phase having the ordered L12 structure (Fig.15 (b)). Figure 16 shows the aluminum and chromium concentration profiles along [100] toward the γ-γ' interface. The aluminum concentration decreases when approaching to the interface, while the chromium concentration increases. This indicates the existence of concentration gradient in the vertical matrix channel across the interface.

Figure 17 shows schematically the position of the analytical volume, which is located at a growing edge of γ' particle and horizontal matrix (γ) channel. The size of the analytical volume is 15nm in diameter and 17nm in height. Figure 18 shows the 3D isosurface representation of the analytical volume in which γ' particle is represented by white and the matrix channel by black. The equi-concentration surfaces are drawn through all points of aluminum concentration at 20at% (γ') and chromium concentration at 25at% (γ). This confirms that the analysis was performed through the interface of the γ' particle and the horizontal matrix channel which is vertical to the external stress as illustrated in Fig.17. Figure 19 shows the 2D atomic mapping representation of a mid-section (5nm thick) sliced from the analytical volume to visualize the arrangement of atoms around the γ-γ' interface. Each spot represents the position of each atom field evaporated. As expected, aluminum atoms partition in the γ' particle, while chromium atoms in the matrix.

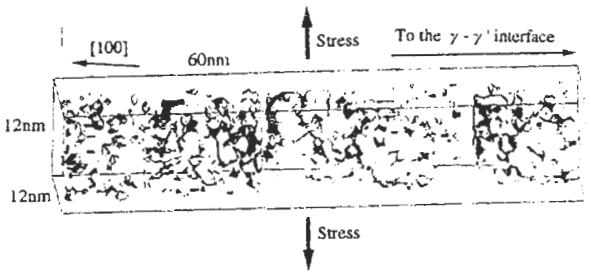

Fig. 14 Isosurface reconstruction showing fine Al-rich domains in the vertical γ phase channel in the early period of directional coarsening. The isosurface is drawn at an aluminum concentration of 20at%

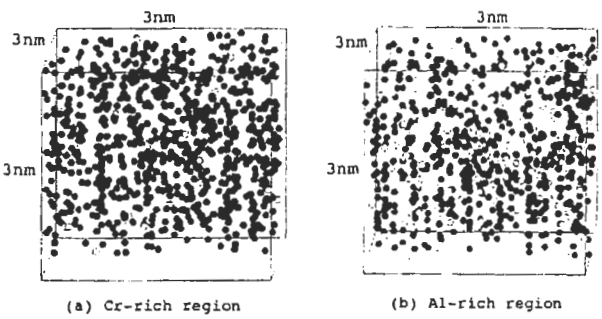

Fig. 15 Atomic distribution of nickel and aluminum in the Al-rich and Cr-rich domains in the vertical γ phase channel (Aluminum atom is represented by an open sphere and nickel by solid)

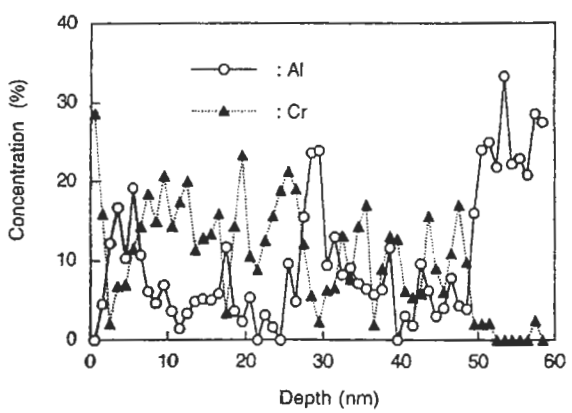

Fig. 16 Aluminum and chromium concentration variations in the vertical γ phase channel. The profiles were taken towards the γ-γ' interface

Compared with these two, molybdenum atoms partition in the matrix and appear to show a slight tendency of segregation in the vicinity of the interface and (Ta+w+Re) atoms show no preference of partitioning. This is reasonable because chromium and molybdenum are known to be γ-stabilizing elements, while aluminum is a γ'-forming element. Concerning the tantalum, tungsten and rhenium atoms it is difficult to distinguish them from each other because of the

mass resolution limitation of the PoSAP. However no clustering or segregation behavior was found for them. It should be also noted that chromium atoms show some segregation around the interface, particularly at the growing edge of the γ' particle.

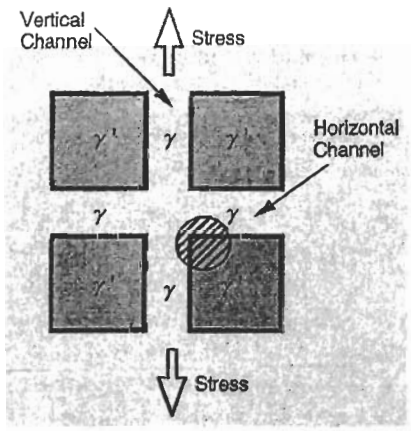

Fig. 17 Location of the PoSAP analytical volume

A comparison of aluminum concentration difference between at the growing edge and in the middle of the γ' particle is made in Fig.20. They are the arbitrary sliced (1nm thick) planes vertical to the [100] and aluminum concentration is represented as gray scale (white ≥ 40at%Al and black ≤ 10at%). Compared with a rather uniform aluminum concentration fluctuation in the bulk, in the vicinity of the γ-γ' interface, aluminum shows some segregation which is not homogeneous but rather localized in several nanometer wide region. This must be an indication of aluminum transport from the horizontal γ-γ' interface to the vertical γ-γ' interface through the growing edge of the γ' particle. The chromium segregation around the edge of the γ-γ' interface may indicate counter flow of chromium atom rejected from the vertical matrix channel which will disappear later because of rafting. This is also supported from aluminum and chromium concentration depth profile across the horizontal and vertical γ-γ' interface as shown in Fig.21. They were obtained by positioning a column of 2nm square cross-section in the analytical volume, one in parallel to the [100] and the other vertical to the [100]. When viewed in terms of chromium concentration profile, the interface broadness is almost the same for both horizontal and vertical interface,

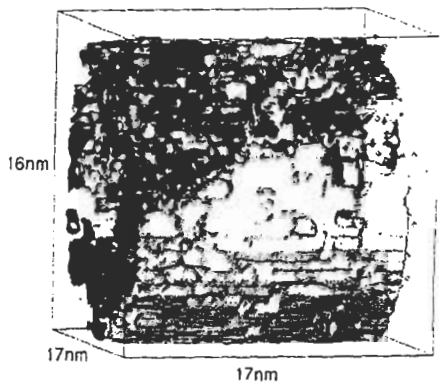

Fig. 18 Isosurface reconstruction showing the γ-γ' interface at the edge of the γ' phase. Gamma phase is represented by black and γ' by white. The isosurface is drawn at 25at%Cr and 20at%Al, respectively

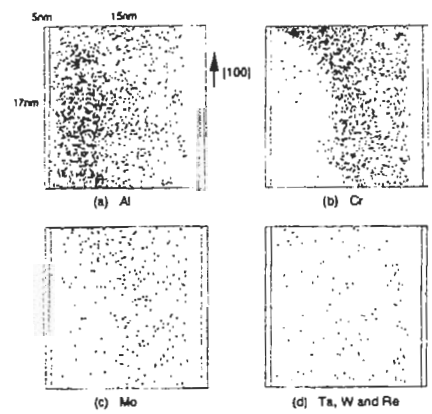

Fig. 19 Atomic distribution of 5nm thick cross-section sliced from the analytical volume (a)Al, (b)Cr, (c)Mo and (d)Ta+w+Re

about 1.6nm. On the other hand, in terms of aluminum concentration profile, the interface is much broader in the horizontal (about 5nm) than in the vertical interface (1.6nm). This may indicate that aluminum mass transport is in progress in the receding horizontal γ-γ' interface during rafting. It should be also noted the presence of high aluminum concentration gradient in the horizontal γ-γ' interface. Furthermore a rather high chromium concentration in the vertical matrix channel may result from the rejection in the growing γ' particle.

A further support for aluminum transport in the interface region can be obtained from the comparison of frequency distribution of aluminum concentration between the bulk and the interface covering the edge area of the γ' particle as shown in Fig.22. It should be noted that there are two peaks of 24at% and 30at% in addition to the peak of 6at% corresponding to the average concentration of the γ phase in γ-γ'

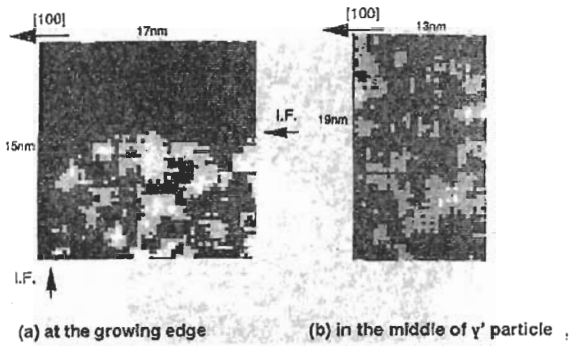

Fig. 20 Comparison of aluminum concentration difference between at the growing edge (a) and in the middle of the γ' particle (b). (Arbitrary sliced cross-section of 1nm thick vertical to [100] and aluminum concentration is represented by gray scale, white is 40at% or higher and black is 10at% or less

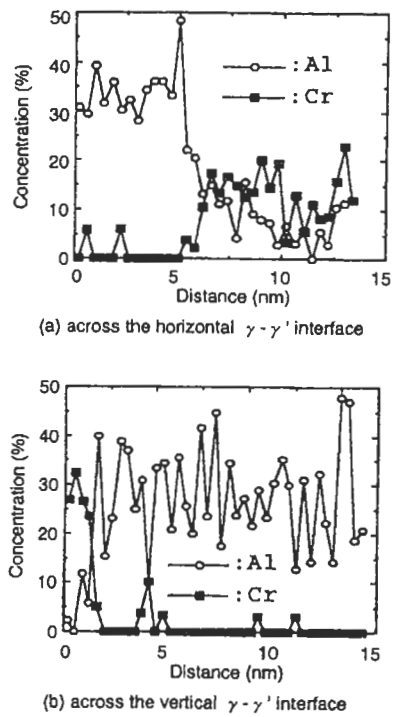

Fig. 21 Comparison of aluminum and chromium concentration profiles between across the horizontal and the vertical γ-γ' interface

interface, while only one peak is found in the bulk of γ' particle (a). This suggests that the fluctuation of aluminum concentration around the edge area of γ' particle increases because of the aluminum diffusion from the horizontal to the vertical interface.

Aluminum diffusion may occur via dislocation or defects in the horizontal γ-γ' interface. High dislocation density is observed in the horizontal interface shown as a TEM micrographs in Fig.23. Through dislocation cores, aluminum atoms diffuse out the horizontal γ-γ' interface,

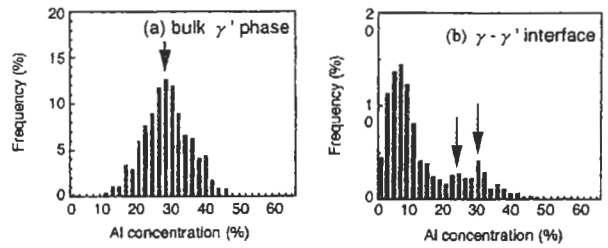

Fig. 22 Comparison of frequency distribution of aluminum concentration between the bulk γ' phase and γ-γ' interface

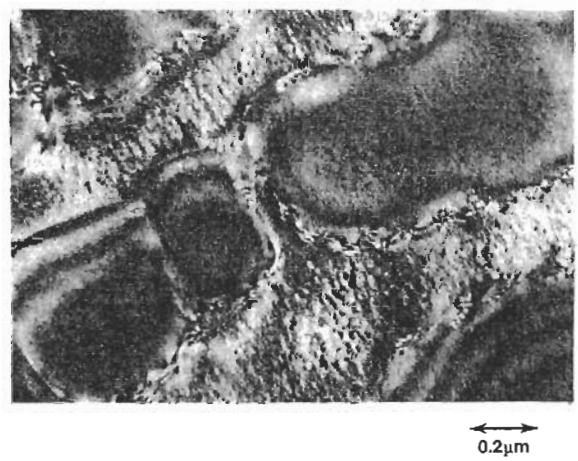

Fig. 23 TEM micrographs showing high dislocation density in the horizontal γ-γ' interface (Courtesy of M.Saito,Hitachi Res.Lab.)

thus resulting in the horizontal interface receding, and diffuse into the vertical channel to evolve as the interconnected structure consisting of finely dispersed γ' precipitates and γ matrix, which is described above. The rafting develops with the growth of the fine precipitates and the movement of the vertical interface. It is assumed that aluminum atoms segregates in a local area in several nanometer size, which may play a sink for the diffused aluminum from the horizontal interface to the vertical interface. This leads to the interface movement when the concentration approaches the equilibrium. Nickel is thermodynamically balanced with aluminum. The other elements diffuse with the interface movement in order to keep the stoichiometry of each phase.

5. Conclusions

The three dimensional atom probe was employed to evaluate the aging degradation process involving diffusional transport of atoms in nanometer scale regions at the atomic level.

1. The true uniqueness of the three dimensional atom probe is demonstrated by the atomic scale visualization of the

fine scale microstructure evolution during the aging process of two structural materials.

2. The ferritic phase of the duplex stainless steel undergoes phase separation during a long term exposure at 450°C, evolving a ultrafine highly interconnected micro-structure consisting of the Cr-enriched and the Cr-depleted domains.
3. Evolution of fine ordered γ' precipitates and their coalescence are observed in the vertical matrix channel of the disordered γ phase surrounded by the ordered cuboidal γ' phase in the early period of high temperature creep of the nickel based superalloy single crystal. This must be the initial step of the directional coarsening of the γ' particles.

Acknowledgment

The authors would like to thank professor G.D.W.Smith and Oxford FIM group for their helpful advice on the PoSAP analysis. They are also grateful to professor H.Kuwano of Muroran Institute of Technology and Dr.T.Ohashi and his coworkers at Hitachi Research Laboratory for their helpful discussion related to the aging process of the stainless steel and the nickel based superalloy.

References

1. A.Cerezo, T.J.Godfrey and G.D.W.Smith : Rev. Sci. Instrum., **59** (1988) 862.
2. D.Blavette, D.Deconihout, A.Bostel, J.M.Sarau, M.Bonet and A.Menand : Rev. Sci. Instrum., **64** (1993) 2911.
3. M.K.Miller : Surf. Sci. **246** (1991) 428.
4. A.Cerezo, T.J.Godfrey, J.M.Hyde, S.J.Sijbrandij and G.D.W.Smith : Appl. Surf. Sci., **76/77** (1994) 374.
5. S.J.Sijbrandij, A.Cerezo, T.J.Godfrey and G.D.W.Smith : Appl. Surf. Sci., **94/95** (1996) 428.
6. A.Cerezo, M.G.Hetherington, J.M.Hyde, M.K.Miller, G.D.W.Smith and J.S.Underkoffler : Surface Sci. **266** (1992) 471.
7. A.Trautwein and W.Gysel : in "Stainless Steel Castings" V.G.Behal and A.S.Melilli eds., ASTM STP 756 (1982) p165.
8. O.K.Chopra and H.M.Chung : in "Properties of Stainless Steels in Elevated Temperature Service" M.Prager ed. MPC-ASME vol.26 (1987) p79.
9. P.H.Pumphrey and K.N.Akhurst : Mater. Sci. Technol. **6** (1990) 211.
10. S.Bonnet, J.Bourgoin, J.Champidonde, D.Guttmann and M.Guttmann : Mater. Sci. Technol. **6** (1990) 221.
11. M.K.Miller and J.Bentley : Mater. Sci. Technol., **6** (1990) 285.
12. Y.Ishikawa and T.Yoshimura : Materials Sci. Forum. **185/188** (1995) 985.
13. T.Yoshimura, Y.Ishikawa, K.Enomoto and S.Sakata : Trans. JSME, A**59** (1993) 2034.
14. T.Yoshimura and Y.Ishikawa : J. Japan Inst. Metals, **56** (1992) 873.
15. M.V.Nathal, R.A.Mackay and R.V.Miner : Metall. Trans., **20A** (1989) 133.
16. R.A.Mackay and M.V.Nathal : micon 86 "Optimization of Processing, Properties, and Service Performance Through Microstructural Control", B.L.Bramfit et.al eds., ASTM STP979, (1988) p201.
17. T.M.Pollock and A.S.Argon : Acta Metall., **42** (1991) 1.
18. T.M.Pollock and A.S.Argon : Acta Metall., **42** (1994) 1859.
19. R.A.Mackay and L.J.Ebert : Metall. Trans., **16A** (1985) 1969.
20. M.Feller-Kniepmeier and T.Link : Metall. Trans., **20A** (1989) 1233.
21. I.L.Svetlov, B.A.Golovko, A.L.Epishin and N.P.Abalakin : Scripta Met., **26** (1992) 1359.
22. T.Yoshimura, Y.Ishikawa, M.Saito, T.Ohhashi and K.Hidaka : Materials Sci. Res. Int. **2** (1996) 13.
23. M.Saito, T.Aoyama, K.Hidaka, H.Tamaki, T.Ohhashi, S.Nakamura and T.Suzuki : Script. Materia. **34** (1996) 1189.